Chapter 5

Preparation and Characterization of Nanostructured TiO_2 Thin Films by Hydrothermal and Anodization Methods

S. Venkatachalam, H. Hayashi, T. Ebina and H. Nanjo

Additional information is available at the end of the chapter

http://dx.doi.org/10.5772/51254

1. Introduction

In recent years, metal oxide materials such as TiO_2 and ZnO thin films have been extensively studied for various applications such as solar cells, gas sensors and protective coating [1-2]. Among them, TiO_2 is a very suitable oxide material for dye-sensitized solar cell (DSC) applications, because of its extraordinary oxidizing ability of photogenerated holes. TiO_2 thin films are prepared by various preparation methods, but the efficiency of the DSC solar cell is strongly enhanced by the increased dye absorption capacity of the photoelectrode. The most important factors which strongly affect the device performance are series resistance, charge carrier-recombination, electron injection from a photoexcited dye into the conduction band of an oxide semiconductor and hole transportation to the counter. Adachi et al. [3] reported that the dye absorption capacity of TiO_2 nanowires was about 4-5 times higher than that of P25 film, which is made of TiO_2 nanoparticles. It means that the electron collection efficiency in P25 film is lower than that of TiO_2 nanowires. The electron collection efficiency is determined by trapping/detrapping events along the site of the electron traps (grain boundaries and defects). All these problems can be resolved using nanostructured TiO_2 films such as nanoholes, nanotubes, nanorods and nanowires. Nanostructured TiO_2 thin films have been prepared by sol-gel, anodization and hydrothermal methods [1, 4]. Very suitable methods to prepare the TiO_2 nanorod and nanotube are hydrothermal and electrochemical anodization. In the present work, TiO_2 nanowires, nanorods, nanoporous and nanotubes were prepared using hydrothermal and anodization methods. In this paper, we report the surface morphological, optical, structural and electrical properties of TiO_2 nanowires, nanorods, nanoporous and nanotubes. The fabrication procedure of dye-sensitized solar cells and the factors which affect the device performance will be discussed. Finally, photovoltaic parameters (I_{sc}, V_{oc}, FF

and η) of DSC based on rutile and anatase TiO_2 films will be compared with TiO_2 nanoporous, nanoholes, nanotube array films based DSC.

2. Experimental methods

TiO_2 nanowires (TNWs), nanorods (TNRs) and nanoporous films were grown on ITO glass substrates using hydrothermal method. The hydrothermal synthesis of TNWs, TNRs and nanoporous was carried out in a Teflon-lined stainless steel autoclave. Titanium n-butoxide (TNB) solution was used as precursor for the production of TiO_2 films. In a typical synthesis process, TNB (0.5 – 1.0 ml) was used with different amounts of HCl (15 - 23 ml), HNO_3 (5 – 15 ml) and deionized water (DI=35-45 ml). Finally, the resulting solution was transferred into an autoclave. Here ITO-coated glass was used as a substrate. The autoclave was sealed and then placed into an electric oven. The synthesis process was carried out for different reaction times as well as temperatures. After completion of the reaction, the autoclave was cooled down to room temperature. Finally, the substrates were thoroughly washed with deionized water, followed by drying overnight at ambient temperature. Nanocrystalline indium tin oxide (ITO) thin films were prepared on glass substrates by ion beam sputter deposition method. The deposition procedure of nanocrystalline ITO thin films can be found elsewhere [5]. The TiO_2 films were characterized by X-ray diffraction (XRD) using Cu Kα radiation (λ=1.54056 Å) at 40 kV and 30 mA, with a Rigaku; RINT 2200VK/PC diffractometer. Transmission through the films was measured using an UV-VIS-NIR spectrophotometer (UV-3150, Shimadzu). The surface morphologies of the TiO_2 films were observed by field emission scanning electron microscopy (FE-SEM, S4800, Hitachi). In order to prepare the DSC devices, the TiO_2 electrodes were immersed in ethanol solution containing N-719 dye. Then the dye-anchored TiO_2 electrodes were rinsed with ethanol solution and dried in air. The liquid electrolyte was prepared by dissolving 0.05 M of iodine (I_2) and 0.5 M of potassium iodide (KI) in 10 ml of ethylene glycol. Meanwhile, platinum film was prepared by ion-beam sputter deposition method and the Pt-sputtered ITO/Glass was used as a counter-electrode. Surlyn spacer film with a thickness of 60 μm was used as a spacer. I-V measurements were performed using Keithley High Resistance Meter/Electrometer 6517A at room temperature.

3. Results and discussion

3.1. Preparation and characterization of TiO_2 thin film by hydrothermal method

The effects of reaction temperature, HCl and titanium n-butoxide (TNB) volume on the structural properties of TiO_2 films are discussed in this section. Here, the volume of titanium n-butoxide (TNB= 1 ml) is fixed and the volume of deionized water (45-30 ml) and HCl (15-23 ml) are varied. The reaction time and temperature are fixed at 17 h and 160° C, respectively.

http://dx.doi.org/10.5772/51254

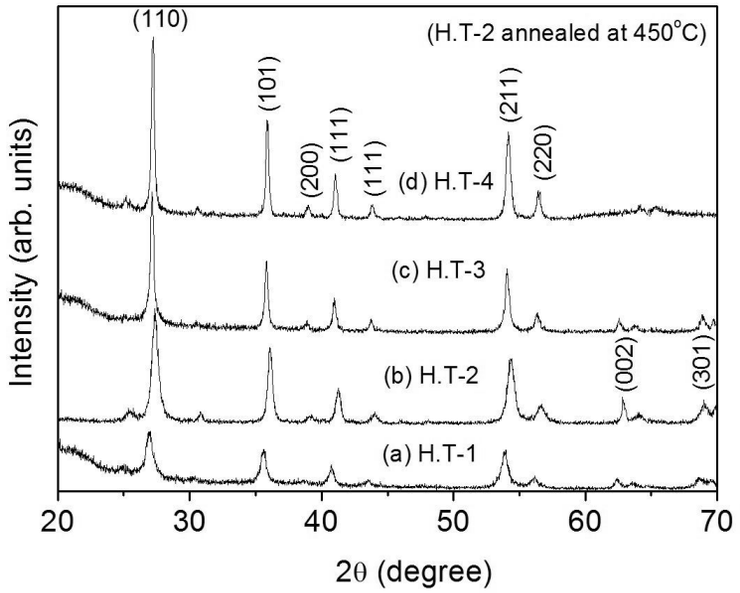

Figure 1. XRD patterns of TiO_2 films prepared using different volume of HCl. (a) H.T-1[HCl=15 ml; DI=45 ml], (b) H.T-2 [HCl=20 ml; DI=40 ml], (c) H.T-3 [HCl=23 ml; DI=30 ml] and (d) H.T-4 [H.T-2 annealed at 450°C for 30 min]. Here TNB (1 ml), reaction time (17 h) and reaction temperature (160°) were kept constant.

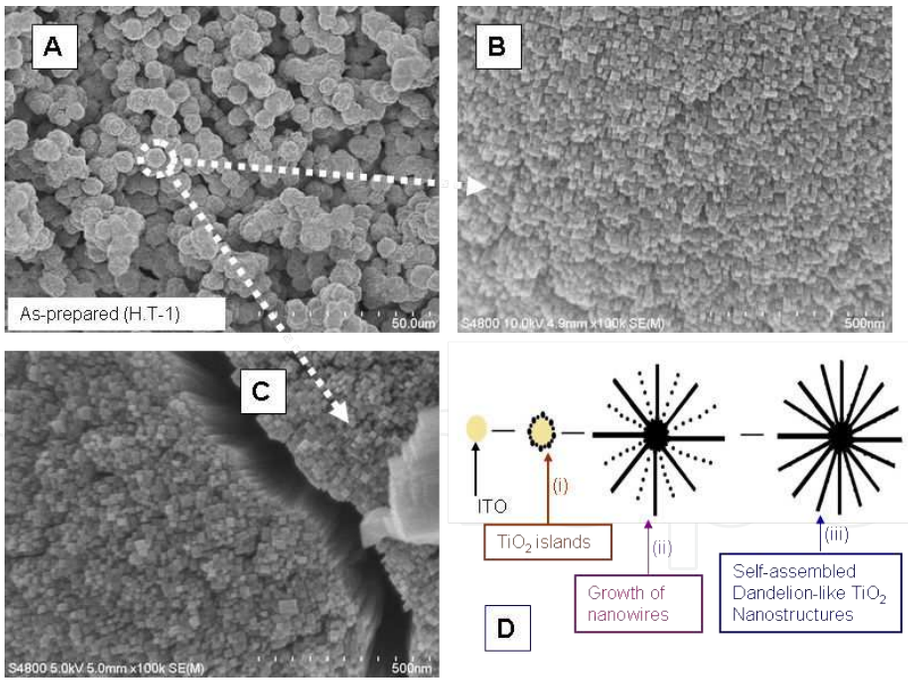

Figure 2. SEM images of TiO_2 films prepared with TNB of 1 ml, HCl of 15 ml, DI of 45 ml, reaction time of 17 h and at a reaction temperature of 160°C.

Figure 1 shows the XRD patterns of TiO_2 films prepared using different volumes of HCl. A very strong rutile peak is observed at 2θ of 27.37°, assigned to (110) plane (see Fig.1). Other

rutile peaks are observed at 2θ of 36.10° (101), 39.16° (200), 41.26° (111), 44.01° (210), 54.36° (211), 56.59° (220), 62.92° (002), 64.10° (310) and 68.91° (301). The (110) peak intensity increases as the volume of HCl is increased from 15 to 23 ml. The positions of all diffraction peaks correspond to rutile TiO_2 and they coincide well with the reported value [6]. However, a weak anatase peak is observed at 2θ of 25.46°, assigned to (101) plane. The TiO_2 sample (H.T-2) is annealed in air at 450°C for 30 min and the XRD pattern of annealed TiO_2 sample is shown in Figure 1(d). The position of these diffraction peaks is the same as those observed in Fig.1 (b). However, the relative intensity of these diffraction peaks increases after annealing at 450°C. This result shows that the increase in HCl volume enhances the growth of the films along (110) direction. This result agrees well with the previous result reported by Wu et al. [7]. Meanwhile, TiO_2 nanorods did not grow on the substrate surface when the volume of HCl is either increased from 23 to 30 ml or decreased from 15 to 10 ml. These data of 10 and 30 ml are not shown in Fig.1. This is attributed that the moderate hydrolysis of titanium n-butoxide (TNB) is important to grow the growth oriented TiO_2 nanorods.

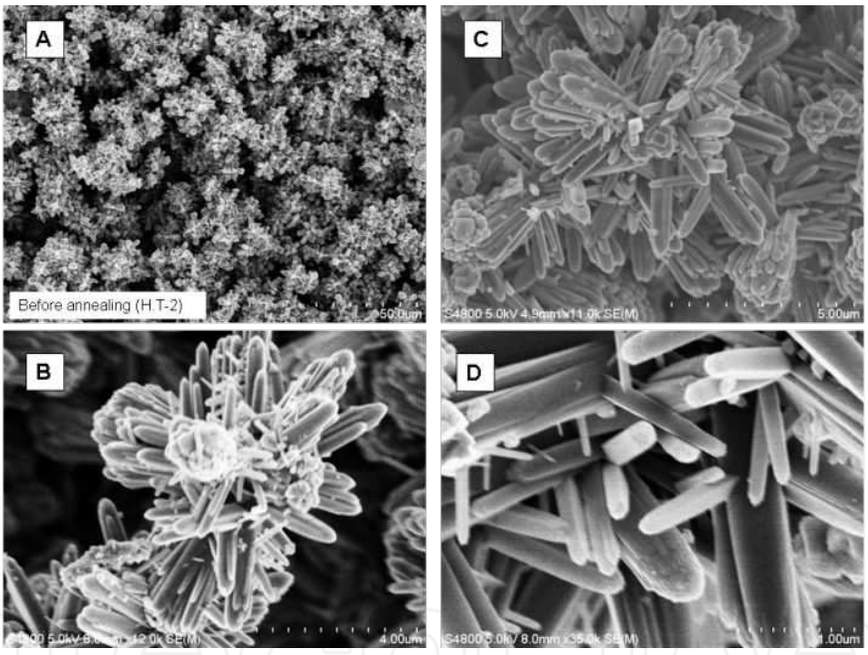

Figure 3. SEM images of TiO_2 films (H.T-2) prepared using TNB of 1 ml, HCl of 20 ml and DI of 40 ml.

Figure 2 shows the SEM images of TiO_2 films prepared on ITO-coated glass substrates with TNB of 1 ml, HCl of 15 ml and DI of 45 ml. The overall morphology indicates the existence of many uniform, dandelion-like TiO_2 nanostructures with diameters in the range of 4 - 6 μm. A selected area of high magnification SEM images [Top (Fig.2B) and side view (Fig.2C)] show that each dandelion-like nanostructure is composed of ordered nanowires with an average diameter of 17 nm. Similar nanowire-structured TiO_2 surface has been observed by Feng et al. [1]. This is attributed that if there is no lattice match between the TiO_2 film and substrate, the TiO_2 firstly nucleated as islands and then nanowires grow from these islands to form dandelion-like morphologies (see the Fig.2d). SEM images of as-prepared TiO_2 films are shown in Fig. 3 which

http://dx.doi.org/10.5772/51254

is prepared by adding HCl volume of 20 ml in the reaction solution. At low and high magnifications (Figs. 3A and B), the whole surface is composed of flower-like structures, which are composed of nanorods and nanorod bundles (see Fig.3C). The nanorod size is in the range of ~150-200 nm (Fig.3D). The as-prepared sample is then annealed at 450°C for 30 min in order to check the robustness of the morphology of the TiO_2 nanorod arrays. The low and high magnification SEM images of annealed TiO_2 films are shown in Figs. 4A and B, respectively. Upon annealing at 450°C, the nanorod array remains unchanged, but the size of the nanorod and nanorod bundles increase after annealing at 450°C (see Fig.4C). After annealing, the size of the nanorod is in the range of 200-300 nm (Fig. 4D). It is apparent that the conversion of nanostructure from nanowires to nanorods is realized by increasing the volume of HCl in the synthesis solution. TiO_2 nanorods did not grow on glass substrates. It seems that the nucleation and growth of the crystals could be promoted by ITO.

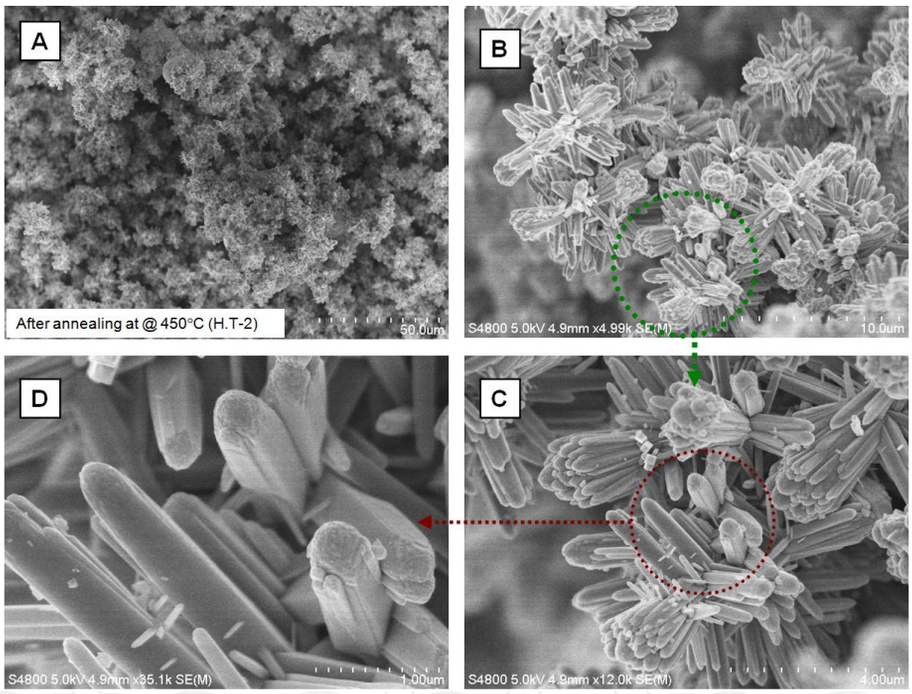

Figure 4. SEM images of TiO_2 films (H.T-2) annealed at 450°C for 30 min.

Figure 5 shows the photocurrent density-voltage characteristics of DSC based on TiO_2 nanowire, nanorod and P25 films. The photovoltaic parameters are given in Table 1. The short-circuit current density and fill factor of nanowire based DSC is higher than that of nanorod based DSC. The optical absorption study shows that the dye absorption capacity of TiO_2 nanowire is much better than that of TiO_2 nanorods (Figure not shown). As a result, the power conversion efficiency of nanowire based DSC is higher that of nanorod based DSC. However, the power conversion efficiency of rutile TiO_2 based DSC is lower than that of anatase TiO_2 (P25) nanoparticles based DSC. Similar results have been observed by Lin et al. [8]. The power conversion efficiency could also be increased by increasing the TiO_2 film thickness [9].

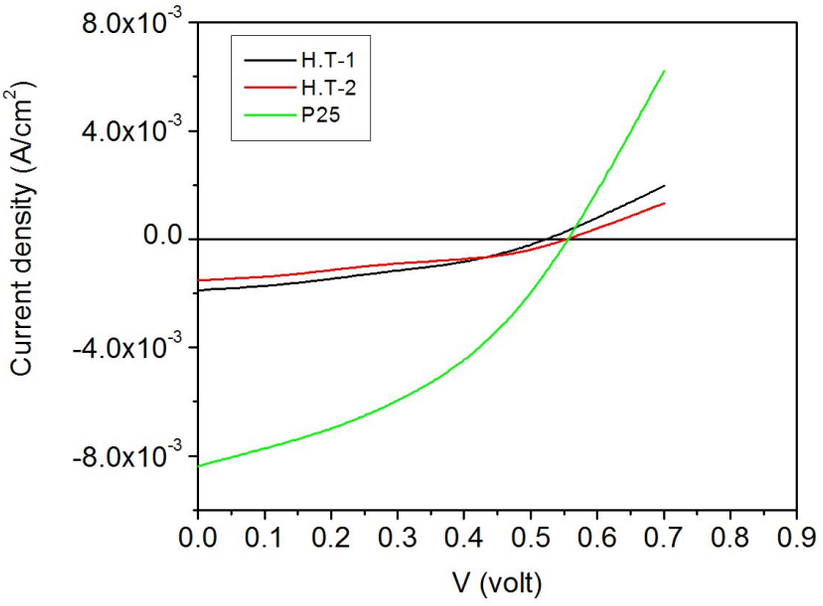

Figure 5. Photocurrent density - Voltage characteristics of TiO_2 nanowires (H.T-1), nanorods (H.T-2) and P25 based DSC for film thicknesses of 4.2 μm (H.T-1), 4.5 μm (H.T-2) and 4.0 μm, respectively.

Photoelectrodes	Film Thicknesses (μm)	V_{oc} (V)	J_{sc} (mA/cm²)	FF	η (%)
TiO_2/ITO (H.T-1)	4.2	0.53	1.88	0.35	0.35
TiO_2/ITO (H.T-2)	4.5	0.56	1.52	0.30	0.25
TiO_2 (P25)	4.0	0.56	8.39	0.41	1.93

Table 1. Photovoltaic parameters of DSC based on TiO_2 nanowires, nanorods and P25 films.

In the above section; effect of HCl concentration on growth rate, surface morphological and structural properties of TiO_2 films is studied. In this section, effect of reaction temperature on the surface morphological and structural properties of TiO_2 films is studied. Figure 6 shows the XRD patterns of TiO_2 films prepared at various reaction temperatures (120 and 160°C). It shows that the rutile phase is dominant (2θ = 27.19°), with weak peaks arising from 2θ values of 35.78° (101), 40.90° (111), 54.03° (211), 56.20° (220) and 62.64° (002) for sample H.T-5. Figure 6b shows the XRD patterns of TiO_2 film prepared at a reaction temperature of 160°C. The XRD intensity of rutile peaks increases as the reaction temperature is increased from 120 to 160°C. This is attributed to the solid state phase transformation [10]. Figure 7 shows the surface morphologies of TiO_2 films prepared at various reaction temperatures. The average diameter and length of TiO_2 nanorod prepared at 120°C are calculated as 125 and 480 nm, respectively. The TiO_2 nanorod length and diameter gradually increases as the reaction temperature is increased from 120 to 160°C. At 160°C, the average diameter and length of TiO_2 nanorods are calculated as 310 nm and 2.6 μm, respectively.

http://dx.doi.org/10.5772/51254

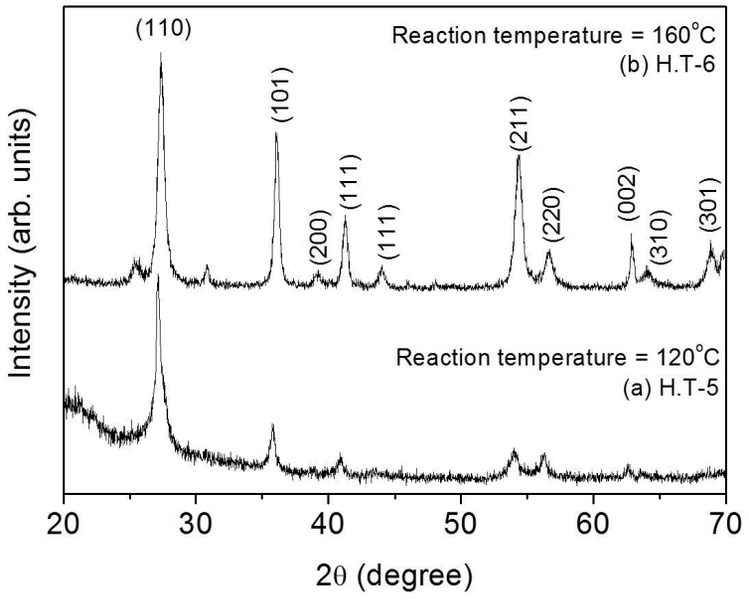

Figure 6. XRD patterns of TiO_2 films prepared at various reaction temperatures (R_T). (a) H.T-5; [R_T=120°C; HCl=20 ml and DI=40 ml] and (b) H.T-6 [R_T=160°C; HCl=20 ml and DI=40 ml]. Here the TNB and reaction time were 1 ml and 17 h, respectively.

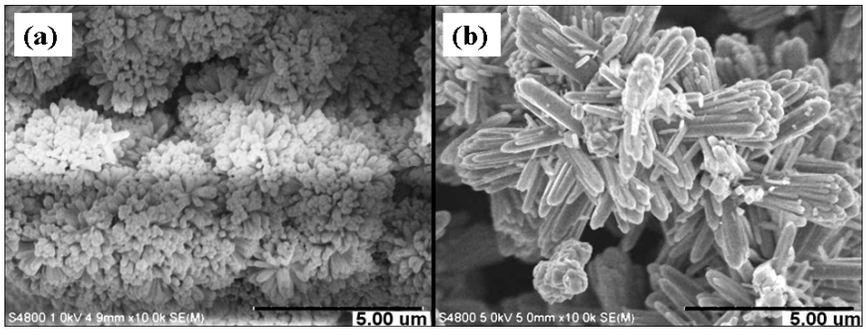

Figure 7. SEM images of TiO_2 films prepared at various reaction temperatures (R_T). (a) H.T-5; [R_T=120°C; HCl=20 ml and DI=40 ml] and (b) H.T-6 [R_T=160°C; HCl=20 ml and DI=40 ml]. Here the TNB and reaction time were 1 ml and 17 h, respectively.

XRD patterns of TiO_2 films prepared using different volume of TNB are shown in Fig. 8. The rutile phase appears to be the dominant phase, with peaks appearing at 2θ values of 27.16° (110), 35.89° (101), 38.94° (200), 41.02° (111) and 43.87° (210) for sample H.T-7 which is prepared at 0.5 ml of TNB. A very small weak anatase phase is also observed at 25.1°, assigned to (101) (see inset of Fig.8). The peak position and FWHM are measured by curve fitting using Gaussian line shape analysis. As the TNB volume is increased to 0.75 ml, a significant change is observed in the XRD pattern of sample H.T-8. But rutile is the dominant phase (Fig.8b). At TNB volume of 1 ml (Fig.8c), two anatase peaks are observed at 25.16° (101) and 53.81° (105). The anatase peak (101) intensity increases as the volume of TNB is increased from 0.5 to 1.0 ml. TiO_2 is grown as a mixture of anatase and rutile, but the rutile phase is

dominant with peaks arising from the (110), (101) and (111) planes. The fraction of anatase can be calculated from the following relation [11]

$$f_a = \left(1 + 1.26\frac{I_r}{I_a}\right)^{-1} \quad (1)$$

where I_a and I_r are the peak intensities of the strongest (101) and (110) reflections of anatase (I_a) and rutile (I_r), respectively. The variations of anatase fractions is shown in Table 2.

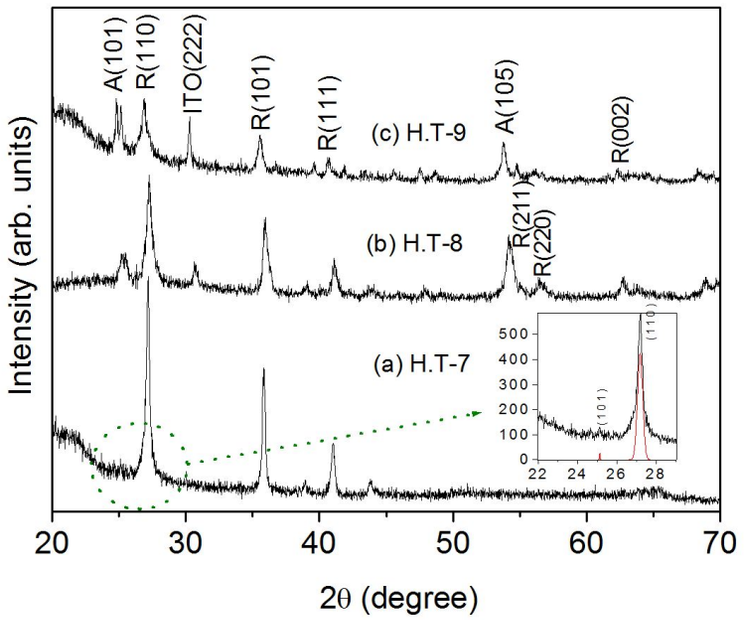

Figure 8. XRD patterns of TiO_2 films grown with three different volume of titanium precursor. (a) H.T-7; [TNB=0.5 ml; HCl=20 ml and DI=40 ml] and (b) H.T-8 [TNB=0.75 ml; HCl=20 ml and DI=40 ml] and H.T-9 [TNB=1.0 ml; HCl=20 ml and DI=40 ml]. Here the reaction time (17 h) and reaction temperature (150°C) were kept constant.

Sample Code	TNB (ml)	HCl (ml)	Di (ml)	I_{101} (a. u)	I_{110} (a. u)	f_a	2θ (degree)	β_{110}	a_{110} (Å)	Stress (%)
H.T-7	0.50	40.0	20.0	13.78	531.72	0.02	27.166	0.23	4.6368	0.89
H.T-8	0.75	40.0	20.0	52.57	207.45	0.17	27.268	0.33	4.6210	0.56
H.T-9	1.00	40.0	20.0	99.30	102.61	0.43	26.906	0.45	4.6826	1.90

Note: TNB – titanium butoxide; HCl– Hydrochloric acid; DI- deionized water; I_{101}-XRD intensity of (101) plane; I_{110}-XRD intensity of (110) plane; f_a-anatase fraction ratio; β_{110}-FWHM of (110) plane; a_{110}-lattice constant.

Table 2. Growth and structural parameters of TiO_2 films.

As shown in Table 2, the fraction of anatase phase increases as the TNB volume is increased from 0.5 to 1.0 ml. It is clear that the phase transformation occurs more easily at low volume of

http://dx.doi.org/10.5772/51254

TNB [10]. The lattice constant of TiO_2 films (Table 2) is greater than that of bulk TiO_2 (4.59 Å) [12]; it is due to the internal stress in the film. The stress in the film is also calculated [5] and is given in Table 2; it shows that all the TiO_2 films prepared under the above mentioned deposition conditions are under tensile stress (Table 2). Surface morphologies of TiO_2 films prepared using different volume of TNB are shown in Fig. 9. SEM images of TiO_2 films prepared under the above mentioned preparation conditions show similar surface morphology. The diameter of the TiO_2 nanorod prepared at 0.5 ml of TNB volume is calculated as 340 nm. The diameter of TiO_2 nanorod is calculated as 240 and 205 nm for 0.75 and 1.0 ml of TNB, respectively.

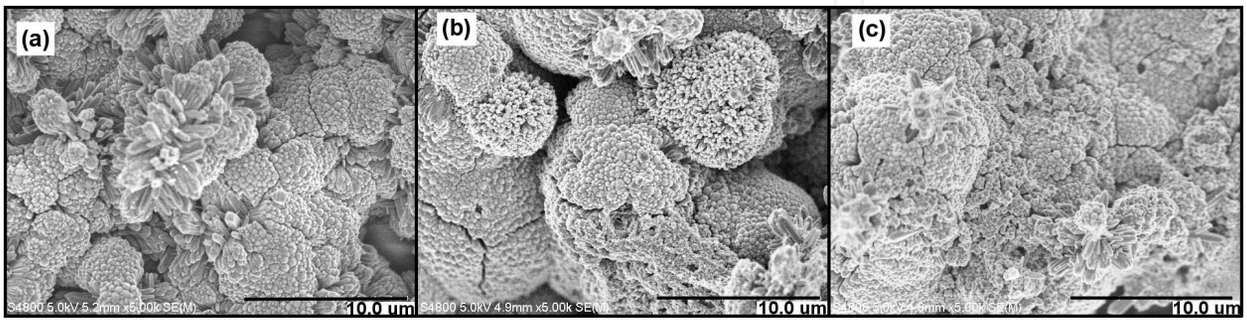

Figure 9. SEM images of TiO_2 films grown with three different volume of titanium precursor. (a) H.T-7, (b) H.T-8 and (c) H.T-9. Here the reaction time (17 h) and reaction temperature (150°C) were kept constant.

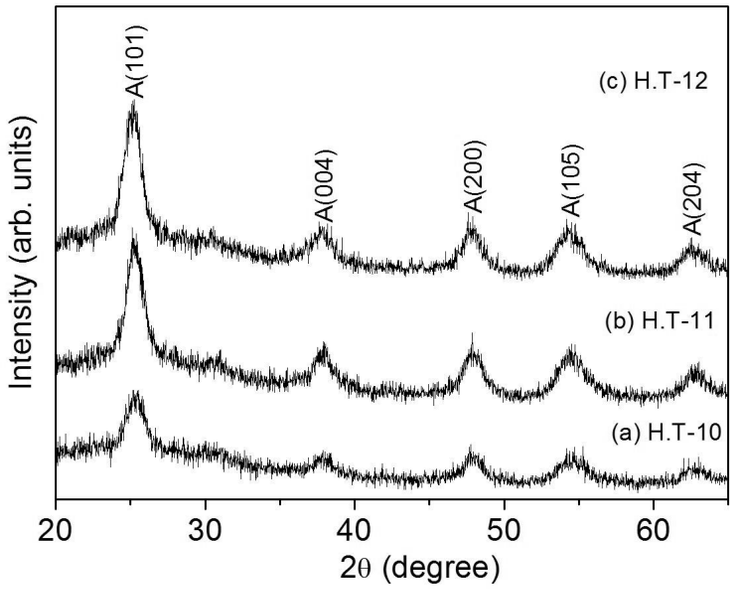

Figure 10. XRD patterns of TiO_2 films prepared using various amounts of HNO_3. (a) HT-10 [HNO_3 =5 ml], (b) H.T-11 [HNO_3=10 ml] and (c) H.T-12 [HNO_3=15 ml]. Here TNB (1 ml), DI (45 ml), reaction time (16 h) and reaction temperature (150°C) were kept constant.

Figure 10 shows the XRD patterns of nanoporous TiO_2 films prepared at various volumes of HNO_3. Here the volume of DI and TNB were fixed at 45 and 1 ml, respectively. Anatase is

the dominant phase in this sample. The TiO_2 sample shows a preferred orientation in the (101) direction, as indicated by strong characteristic peak at 2θ = 25.34°. Some anatase peaks appear at 2θ of 37.92° (004), 47.90° (200), 54.55° (105) and 62.4° (204). The anatase phase remains as the dominant phase in HNO_3 volume of 5, 10 and 15 ml. In all the cases, a pure anatase phase is observed with characteristic peaks at 25.14° (101), 37.78° (004), 47.86° (200), 54.42° (105) and 62.62° (204). This result shows that HNO_3 is very suitable to grow anatase TiO_2 on ITO coated glass substrates. It is concluded that the addition of HCl strongly enhances the growth of the film along (110) direction. In contrast, HNO_3 solution enhances the film growth in (101) direction. In the hydrothermal process, Cl^- and NO_3^- anions play an important role in the formation of rutile and anatase TiO_2 films, respectively. Because NO_3^- anions show stronger affinity to titanium than Cl^-, the pure anatase TiO_2 could be easily obtained in HNO_3 medium.

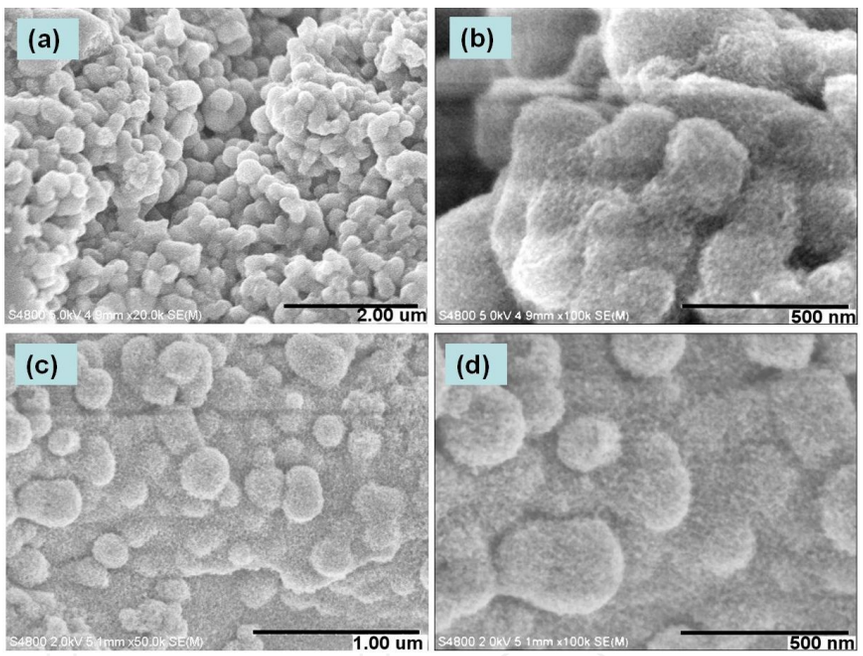

Figure 11. Low and high magnification SEM images of TiO_2 films prepared using various amounts of HNO_3. (a) HT-10 [HNO_3 =5 ml] and (b) H.T-11 [HNO_3=10 ml]. Here TNB (1 ml), DI (45 ml), reaction time (16 h) and reaction temperature (150°C) were kept constant.

Figure 11 shows the surface morphologies of nanoporous TiO_2 films prepared at various volumes of HNO_3. Here the volume of DI and TNB were fixed at 45 and 1 ml, respectively. SEM images clearly show the formation of nanoporous TiO_2 films on ITO coated glass substrates. For DSC applications, the TiO_2 coated ITO sample was annealed at 270°C for 1 h under a vacuum of 90 kPa. The nanoporous TiO_2 film thicknesses are calculated as ~3 and 3.2 μm for HNO_3 volume of 5 and 10 ml. Finally, the TiO_2 electrodes were immersed into the ethanol solution containing N-719 dye. Then the dye-anchored TiO_2 electrodes were rinsed with ethanol solution and then dried in air. Figure 12 shows the photocurrent density-voltage characteristics of DSC based on nanoporous TiO_2/ITO. The short circuit density of TiO_2

http://dx.doi.org/10.5772/51254

electrode based DSC increases from 4.02 to 5.9 mA/cm² as the nanoporous TiO_2 film thickness is increased from 3 to 3.2 μm. The fill factor and power conversion efficiency also increase with increasing nanoporous TiO_2 film thickness (see Table 3).

Photoelectrode	Film Thickness (μm)	V_{oc} (V)	J_{sc} (mA/cm²)	FF	η (%)
TiO_2/ITO (H.T-10)	3.0	0.40	4.02	0.512	0.82
TiO_2/ITO (H.T-11)	3.2	0.38	5.90	0.534	1.20

Table 3. Photovoltaic parameters of DSC based on TiO_2 nanoporous films.

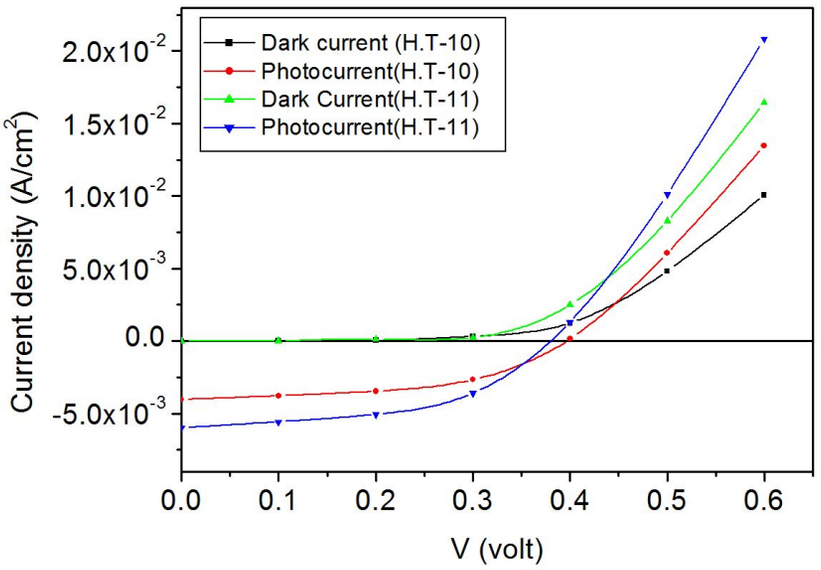

Figure 12. Photocurrent density –voltage characteristics of TiO_2 nanoporous based DSC for different film thickness (3.0 μm (H.T-10) and 3.2 μm (H.T-11)).

3.2. Preparation and characterization of TiO_2 thin films by electrochemical anodization method

Nanocrystalline ITO thin films were deposited on glass substrates by ion beam sputter deposition method at room temperature. The applied acceleration voltage was 2500 V. The sputtering process was performed in 3%O_2 + Ar gas. The gas flow rate was controlled by mass flow meter. Ti thin films were deposited on ITO coated glass substrate by ion beam sputter deposition method at room temperature. The acceleration voltage supplied to the main gun was fixed at 2500 V. Pure Ar was employed as the sputtering gas. The electrochemical anodization was performed in 1M H_2SO_4+0.15 wt. % HF at an applied potential of 10 V for different anodization time (30, 60 and 120 min). Nanostructured TiO_2 films were formed by anodization using a two-electrode configuration with Ti film as an anode and platinum electrode as a cathode. The anodized Ti sample was then annealed in air at 450°C for an hour.

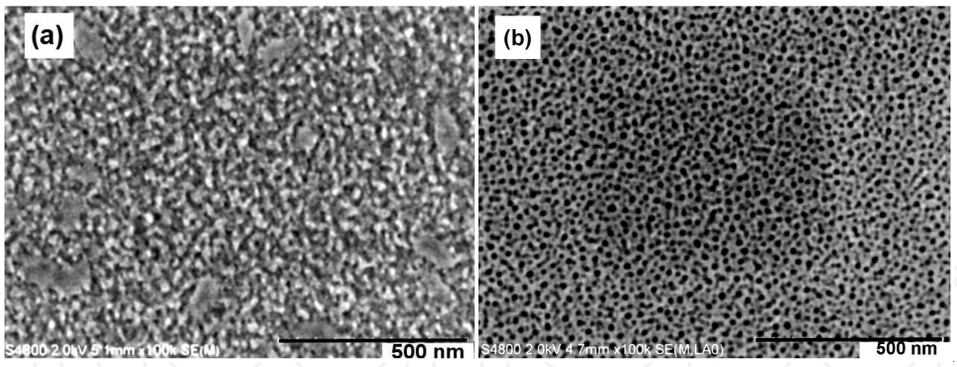

Figure 13. SEM images of TiO_2 films; a) 30 min (T-1) and (b) 60 min (T-2).

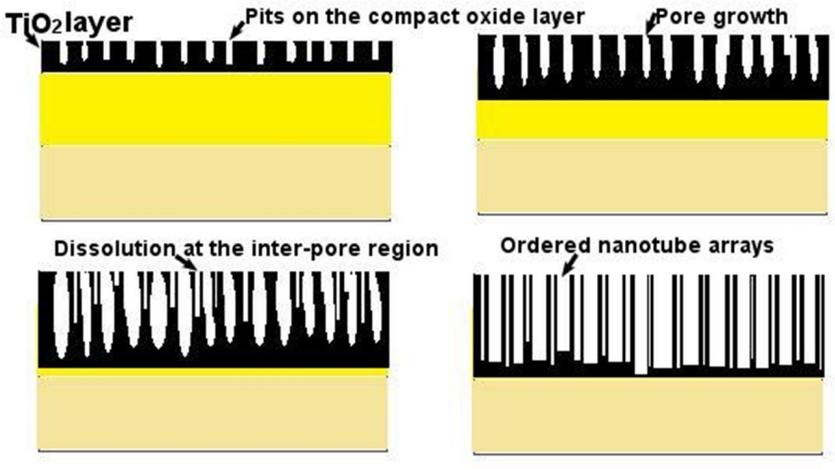

Figure 14. Schematic diagram of the growth stages of TiO_2 nanotube arrays by anodization.

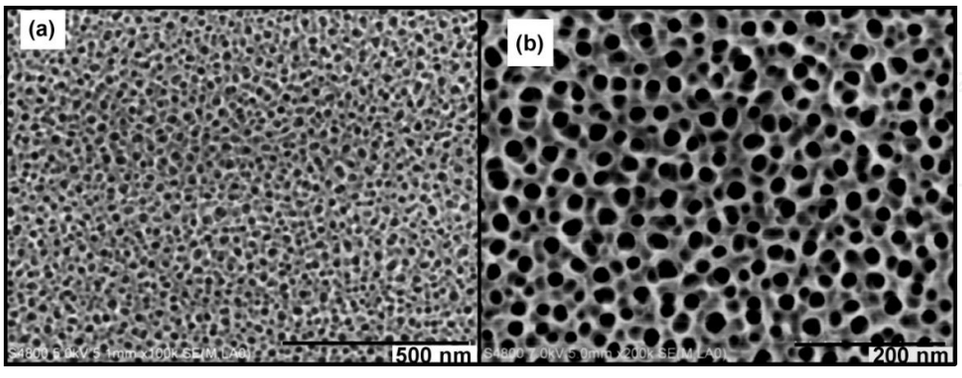

Figure 15. Low (a) and high (b) magnification SEM images of Ti plate anodized at an applied potential of 10 V.

Figure 13 shows the top-view SEM images of anodized Ti films in H_2SO_4/HF electrolytes at an applied potential of 10 V for anodization time of 30 min (Fig.13a) and 60 min (Fig.13b),

http://dx.doi.org/10.5772/51254

respectively. It can be seen that TiO_2 nanoporous were formed when the anodization time was fixed at 30 min (see Fig.13a). When the anodization time was increased to 60 min, highly ordered TiO_2 nanoporous arrays were formed (see Fig.13b). Similar results have been observed by Huang et al. [13]. Generally, the formation mechanism of the TiO_2 nanoporous arrays is proposed as two competitive processes; electrochemical oxidation and chemical dissolution. From these results, we observed that no TiO_2 nanotubes, but TiO_2 nanoporous were formed at the anodization time of 60 min. It shows that the TiO_2 porous layer is easily formed during the short-time of anodization. TiO_2 nanotube arrays can also be prepared on the Ti film surface, but this can be accomplished by increasing the anodization time; this is due to the high chemical dissolution at the inter-pore region (see Fig.14c& d). Because of the limitation of Ti film thickness, Ti metal was used in order to check this effect. Figure 15 shows surface morphology of anodized Ti plate for 120 min. It can be seen that the pore growth and formation on the Ti surface were uniformly distributed (Fig. 15a). It clearly shows the formation of pore growth and small opening at the inter-pore region (Fig. 15b). Similar results have been observed by Yang et al. [14] and Kaneco et al. [15]. Figure 14c can be correlated with Fig.15b. These results clearly show that high dissolution rate at the inter-pore region is very important in order to get the ordered nanotube arrays (see Fig. 14d).

Figure 16 shows the current density-time transient curve recorded during the anodization of Ti sample at an applied potential of 10 V for 30 min. Initially, the current density gradually increases (see inset of Fig.16) because of the electrochemical treatment which consists of a potential ramp from 0 to 10V with a sweep rate of 50 mV/sec followed by a constant potential at 10 V for 30 min. Once the oxide layer is formed, the impedance between the electrodes increases; which results in a drastically reduced current between the electrodes. Furthermore, there is no change in impedance.

Figure 17 shows the optical transmittance spectrum of titania films after annealing at 450°C for an hour. The optical transmittance of annealed nanoporous TiO_2 film in the visible range is estimated as 60%. The thickness of nanoporous TiO_2 film can be calculated from the following relation:

$$d = \frac{\lambda_1 \lambda_2}{2[\lambda_2 n(\lambda_1) - \lambda_1 n(\lambda_2)]} \tag{2}$$

where n (λ_1) and n(λ_2) are the refractive indices of the two adjacent maxima (or minima) at λ_1 and λ_2. The film thickness of TiO_2 is calculated as 250 nm. The relation between absorption coefficient α and incident photon energy hν can be written as [16].

$$\alpha h\nu = C(h\nu - E_g{}^d)^{1/2} \tag{3}$$

for a direct allowed transition, where C is constant and $E_g{}^d$ is direct band gap. The plot of hν vs. $(\alpha h\nu)^2$ is shown in Fig.18. The optical band gap is calculated as 3.25 eV. The optical band gap of nanoporous TiO_2 film is little bit greater than that of bulk anatase TiO_2 (3.2 eV). Similar band tail (2.66 eV) at the low energy side has been observed by Mor et al. [17]. The refractive index

was calculated from the measured transmittance spectrum. Figure 19 shows the variation refractive index versus wavelength of nanoporous TiO_2 film after annealing at 450°C for an hour. It shows that the refractive index gradually decreases with increasing wavelength. The porosity of nanoporous TiO_2 films can be calculated from the following relation [17]

$$Porosity(\%) = \left[1 - \frac{n^2 - 1}{n_d{}^2 - 1}\right] \times 100 \tag{4}$$

where n and n_d are the refractive indices of the nanoporous film (2.2) and non-porous anatase film (2.5), respectively. The porosity of nanoporous structure is calculated as 27 %.

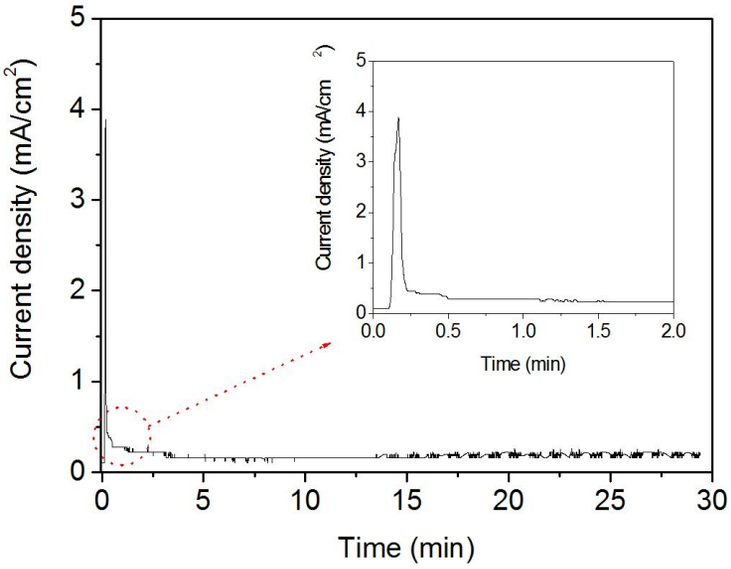

Figure 16. The current density vs. time transient curve which was recorded during the anodization of Ti film for an anodization time of 30 min.

Figure 20 shows the dark and photocurrent density versus voltage characteristics of DSC solar cells based on nanoporous titania films. The power conversion efficiencies of device-1 (T-1) and 2 (T-2) are calculated as 0.25 and 0.17 %. Similar results have been observed by Yang et al. [14]. The short-circuit current density of device-2 is higher than that of device-1. SEM images (T-1 and T-2) show that the TiO_2 films have different surface morphology; due to this, the DSC devices show difference in performance; because the amount of dye adsorption can be increased by large internal surface area of the films. The fill factor and open circuit voltage of device-1 are higher than that of device-2. It shows that the fill factor can be affected by resistance of the substrate and quality of the counter electrode. In the present work, Pt coated ITO films were used as counter electrodes. The low value of fill factor is attributed to large large value of series resistance at the interface between TiO_2 and ITO films. Figure 21 shows the dark and photocurrent density-voltage characteristics of TiO_2/Ti plate. The power conversion efficiency of device-3 is estimated as 0.01% (see Table 4). This result agrees well with the previous results

http://dx.doi.org/10.5772/51254

reported by Ok et al. [18]. The power conversion efficiency of device-3 is much lower than that of device-1 and device-2 (see Table 4). Particularly, the short-circuit current for device-3 is much lower than that of device-1 and 2. It is attributed that the backside illumination affects the light absorption capacity of the dyes, because the I_3^- electrolyte cuts the incident light in the wavelength range from 400 – 650 nm. But the fill factor for device-3 is higher than that of device-1 and device-2. It shows that the high value of FF is attributed to the small value of series resistance at TiO_2/substrate interface.

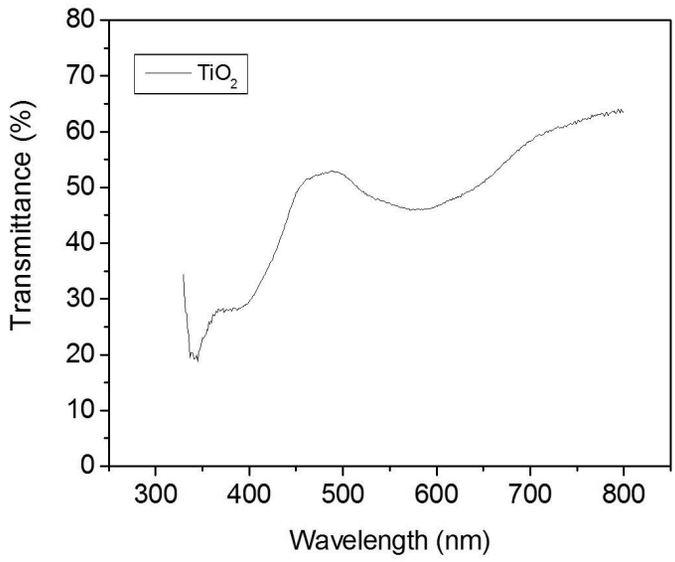

Figure 17. Optical transmittance spectrum of nanoporous TiO_2 film after annealing at 450°C.

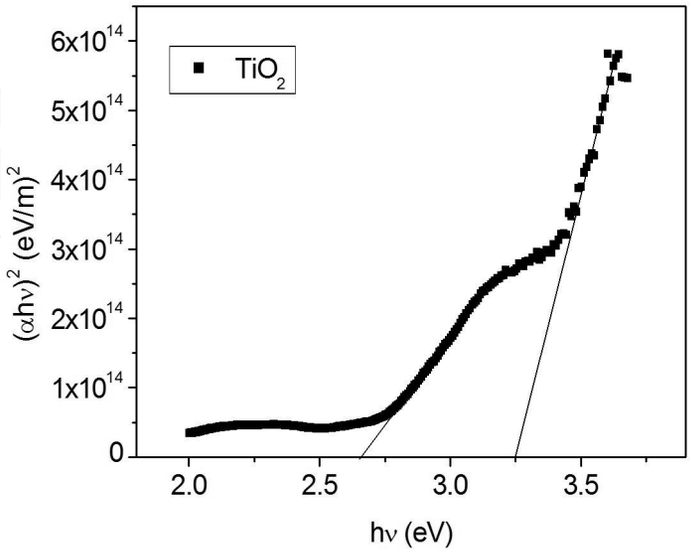

Figure 18. Plot of hν vs. $(\alpha h\nu)^2$ of nanoporous TiO_2 film after annealing at 450°C.

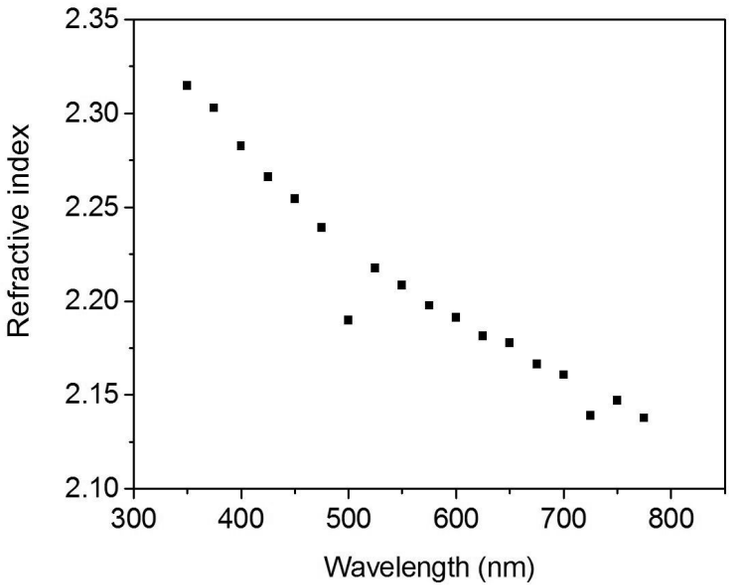

Figure 19. Variation of refractive index of annealed nanoporous TiO_2 film. The average refractive index of nanoporous structure in the visible range is 2.2.

Photoelectrode	Film Thickness (nm)	Voc (V)	Jsc (mA/cm²)	FF	η (%)
TiO_2/ITO/Glass	250	0.432	1.58	0.36	0.25
TiO_2/ITO/Glass	350	0.358	1.72	0.28	0.17
TiO_2/Ti plate	-	0.482	0.07	0.39	0.01

Table 4. Photovoltaic parameters of DSC based on TiO_2 nanoporous films.

Nanostructured TiO_2 was prepared by anodization of Ti foil at room temperature. The anodization was performed in ethylene glycol containing 2 vol.% H_2O+ 0.3 wt.% NH_4F for an anodization of 180 min at 30 V. The anodized Ti sample was then annealed in air at 400°C for an hour. Figure 22 shows surface morphologies of anodized Ti foil. It clearly shows the formation of well ordered TiO_2 nanotube arrays on Ti foil (Fig. 22a). At the bottom, the nanotubes are closely packed together (Fig. 22b). The diameter and wall thickness of TiO_2 nanotube arrays are calculated as 45 nm and 25 nm, respectively. The length of TiO_2 nanotube arrays is estimated as 4.5 μm (Fig. 22c). The side-view of the tube layer (Fig. 22d) reflects an uneven morphology. Figure 23 shows the XRD patterns of anodized Ti foil before and after annealing. In Fig. 23a, the XRD peaks at 35.3, 38.64, 40.4, 53.2 and 63.18 correspond to Ti. This is attributed that the as-prepared TiO_2 is amorphous before annealing; only Ti peaks are seen (Fig. 23a). In order to change the amorphous TiO_2 into anatase TiO_2, anodized Ti sample was annealed in air at 400°C for an hour. After annealing, the amorphous TiO_2 has been changed into crystalline with a more preferred orientation along (101) direction.

http://dx.doi.org/10.5772/51254

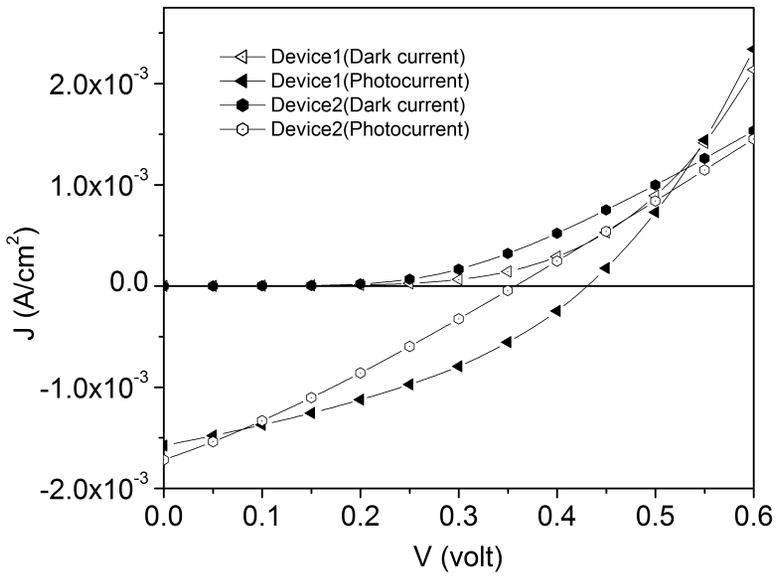

Figure 20. Dark and photocurrent density versus voltage characteristics of DSC based on nanoporous titania films.

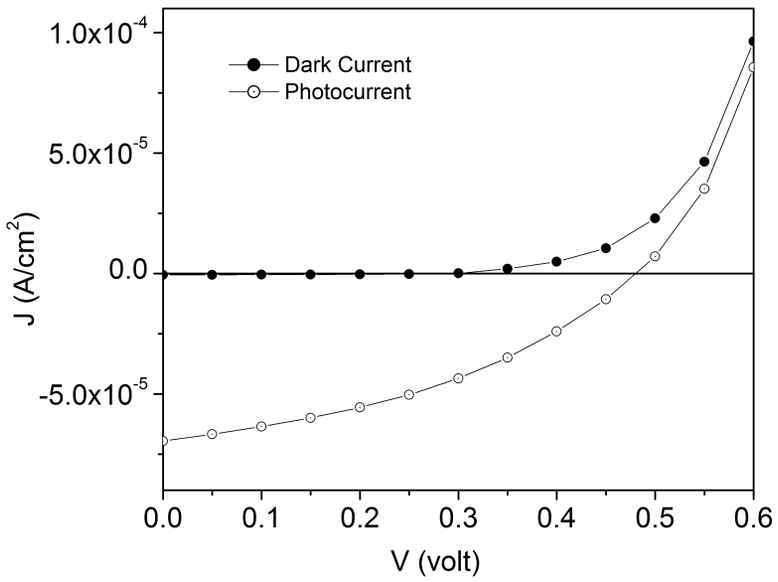

Figure 21. Dark and photocurrent density– voltage characteristics of TiO_2/Ti plate (Device 3).

Figure 24 shows the photocurrent density-voltage characteristics of DSC based on TiO_2 nanotubes arrays. Under back-side illumination, the open circuit voltage, short-circuit current density, fill-factor and power conversion efficiency of DSC based on TiO_2 nanotube arrays are estimated as 0.55 V, 8.27 mA/cm^2, 0.39 and 1.78 %, respectively. Similar results have

been observed by Tao et al. [19]. This result shows that the main factor responsible for enhancement of short circuit current is improvement of electron transport and electron lifetime in TiO_2 nanotube arrays. This increased light-harvesting efficiency in TiO_2 nanotube-based DSC could be a result of stronger light scattering effects that leads to significantly higher charge collection efficiencies of nanotube-based DSC.

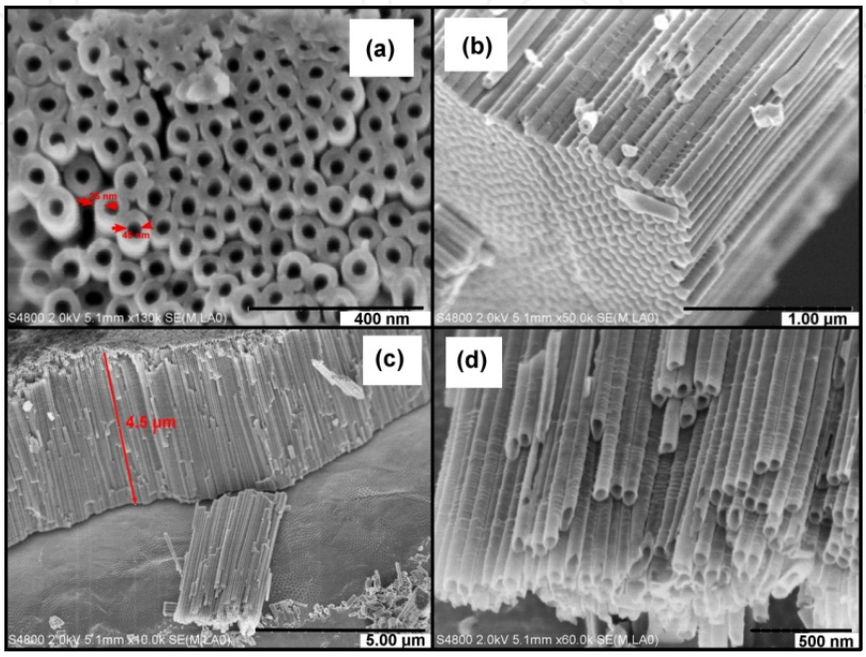

Figure 22. SEM images of Ti foil anodized at an applied potential of 30 V.

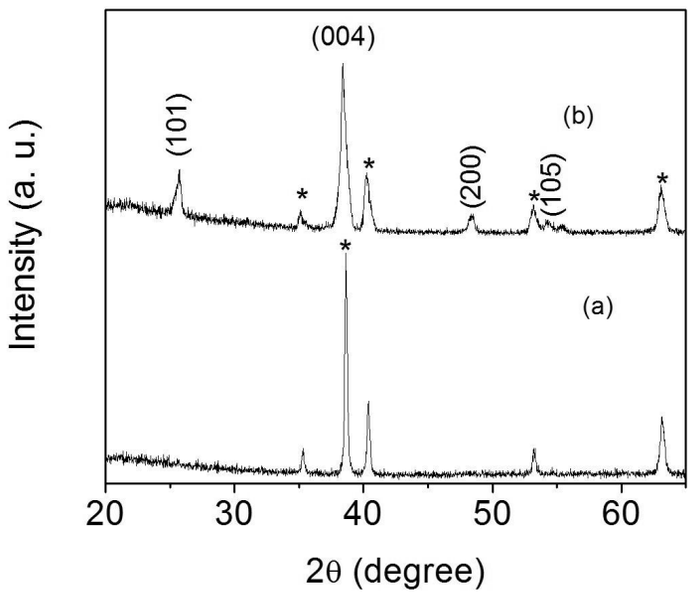

Figure 23. XRD patterns of as-prepared (a) and annealed (400°C) TiO_2 nanotube arrays.

http://dx.doi.org/10.5772/51254

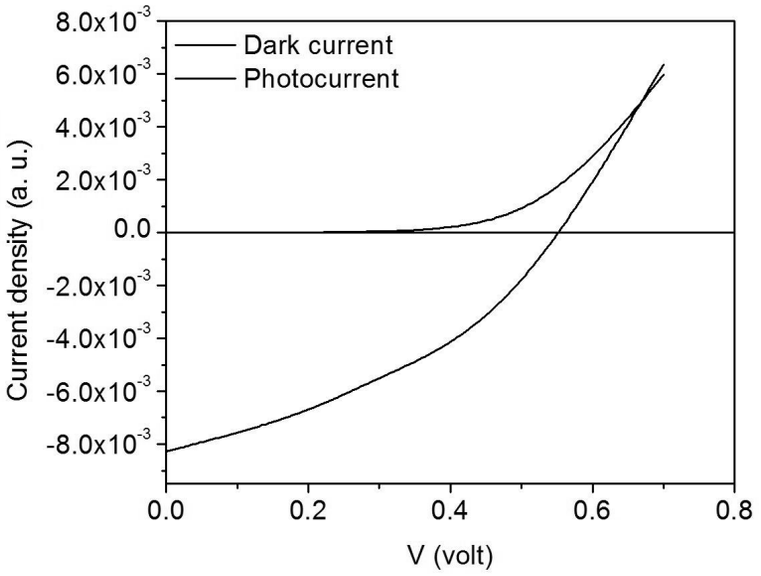

Figure 24. Dark and photocurrent density-voltage characteristics of TiO_2 nanotube arrays.

4. Conclusions

TiO_2 nanowires, nanorods and nanoporous films were successfully prepared using hydrothermal method. The nanorod size increased as the volume of HCl in the reaction solution was increased. Annealing at 450°C for 30 min produced no substantial change in the structure. A rutile to anatase phase transition was observed when the TNB volume increased from 0.5 to 1.0 ml. From the XRD patterns, no rutile structure peaks was detected for the films grown in HNO_3 medium. In this case, anatase was the dominant phase. XRD clearly showed that the crystal quality and orientation of final products were strongly dependent on the experimental parameters, such as volume of TNB, HCl and HNO_3 solution and the reaction temperature. The shape and size of the nanowires and nanorods could be perfectly generated by controlling the volume of HCl and the annealing temperature. Photovoltaic parameters showed that the power conversion efficiency of DSC based on anatase TiO_2 was higher than that of rutile TiO_2 based DSC. TiO_2 nanoporous, nanoholes and nanotubes were successfully fabricated by anodization method. The power conversion efficiency of TiO_2 nanoporous and nanotube arrays based DSC was higher than of TiO_2 nanohole based DSC. The device performance of nanoporous TiO_2 films prepared on transparent conducting substrate was higher than that of TiO_2 nanoholes on Ti plate. The front-side illumination was very suitable in increasing the light harvesting efficiency of the solar cell device.

Author details

S. Venkatachalam*, H. Hayashi, T. Ebina and H. Nanjo

*Address all correspondence to: svchalam23@gmail.com

National Institute of Advanced Industrial Science and Technology (AIST), Sendai, Japan

References

[1] Feng, X., Shankar, K., Varghese, O. K., Paulose, M., Latempa, T. J., & Grimes, C. A. (2008). Vertically Aligned Single Crystal TiO_2 Nanowire Arrays Grown Directly on Transparent Conducting Oxide Coated Glass: Synthesis Details and Applications. Nano. Lett. . http://pubs.acs.org/doi/abs/10.1021/nl802096a , 8, 3781-3786.

[2] Baxter, J. B., Walker, A. M., Van Ommering, K., & Aydil, E. S. (2006). Synthesis and characterization of ZnO nanowires and their integration into dye-sensitized solar cells. *Nanotechnology*, 17, S304, http://iopscience.iop.org/0957-4484/17/11/S13/.

[3] Adachi, M., Murata, Y., Takao, J., Jiu, J., Sakamoto, M., & Wang, F. (2004). Highly Efficient Dye-Sensitized Solar Cells with a Titania Thin-Film Electrode Composed of a Network Structure of Single-Crystal-like TiO_2 Nanowires Made by the "Oriented Attachment" Mechanism. J. Am. Chem. Soc. . http://pubs.acs.org/doi/abs/10.1021/ja048068s , 126, 14943-14949.

[4] Yuxiang, L., Mei, Z., Min, G., & Xidong, W. (2010). Hydrothermal growth of well-aligned TiO2 nanorod arrays: Dependence of morphology upon hydrothermal reaction conditions. *Rare metals*, 29, 286-291, http://www.springerlink.com/content/9433284w0142tt58/.

[5] Venkatachalam, S., Nanjo, H., Hassan, F. M. B., Kawasaki, K., Kanakubo, M., Aizawa, T., Aida, T., & Ebina, T. (2010). Characterization of nanocrystalline indium tin oxide thin films prepared by ion beam sputter deposition method. *Thin Solid Films*, 518, 6891-6896, http://dx.doi.org/10.1016/j.tsf.2010.07.034.

[6] Kumar, A., Madaria, A. R., & Zhou, C. Growth of Aligned Single-Crystalline Rutile 2 Nanowires on Arbitrary Substrates and Their Application in Dye-Sensitized Solar Cells. J. Phys. Chem. C . http://pubs.acs.org/doi/abs/10.1021/jp100491h , 114, 7787-7792.

[7] Wu, M., Long, J., Huang, A., & Luo, Y. (1999). Microemulsion-Mediated Hydrothermal Synthesis and Characterization of Nanosize Rutile and Anatase Particles. Langmuir . http://pubs.acs.org/doi/abs/10.1021/la990514f , 15, 8822-8825.

[8] Lin, C.-J., Tu, W.-K., C.-K., Kuo, & Chien, S.-H. Single-step fabrication of phase-controllable nanocrystalline 2 films for enhanced photoelectrochemical water splitting

and dye-sensitized solar cells. J. Power Sources . http://dx.doi.org/10.1016/j.jpowsour.2010.12.077 , 196, 4865-4869.

[9] Tang, X., Qian, J., Wang, Z., Wang, H., Feng, Q., & Liua, G. (2009). Comparison of low crystallinity TiO_2 film with nanocrystalline anatase film for dye-sensitized solar cells. *J. Colloid Interf. Sci.*, 330, 386-391, http://www.sciencedirect.com/science/article/pii/S0021979708013994.

[10] Wu, M., Lin, G., Chen, D., Wang, G., He, D., Feng, S., & Xu, R. (2002). Sol-Hydrothermal Synthesis and Hydrothermally Structural Evolution of Nanocrystal Titanium Dioxide. *Chem. Mater.*, 14, 1974-1980, http://pubs.acs.org/doi/full/10.1021/cm0102739.

[11] Spurs, R. A., & Myers, H. (1957). Quantitative Analysis of Anatase-Rutile Mixtures with an X-Ray Diffractometer. *Anal. Chem.*, 29, 760-762, http://pubs.acs.org/doi/abs/10.1021/ac60125a006.

[12] Tanemura, S., Miao, L., Wunderlich, W., Tanemura, M., Mori, Y., Toh, S., & Kaneko, K. (2005). Fabrication and characterization of anatase/rutile-TiO_2 thin films by magnetron sputtering: a review. *Sci. Tech. Adv. Mater.*, 6, 11-17, http://iopscience.iop.org/1468-6996/6/1/A03.

[13] Huang, L., Peng, F., Yu, H., Wang, H., Yang, J., & Li, Z. (2010). The influence of ultrasound on the formation of TiO_2 nanotube arrays. *Material Research Bulletin*, 45, 200, http://dx.doi.org/10.1016/j.materresbull.2009.09.018.

[14] Yang-J, D., Park, H., Cho-J, S., Kim-G, H., & Choi-Y, W. (2008). TiO_2-nanotube-based dye-sensitized solar cells fabricated by an efficient anodic oxidation for high surface area. *J. Phys. Chem. Solids*, 69, 1272-1275, http://www.sciencedirect.com/science/article/pii/S0022369707006361.

[15] Kaneco, S., Chen, Y., Westerhoff, P., & Crittenden, J. C. (2007). Fabrication of uniform size titanium oxide nanotubes: Impact of current density and solution conditions. *Scripta Mater.*, 56, 373-376, http://www.sciencedirect.com/science/article/pii/S1359646206008025.

[16] Venkatachalam, S., Mangalaraj, D., & Narayandass, Sa. K. (2007). Characterization of vacuum-evaporated ZnSe thin films. *Physica B*, 393, 47-55, http://www.sciencedirect.com/science/article/pii/S0921452606019466.

[17] Mor, G. K., Varghese, O. K., Paulose, M., Ong, K. G., & Grimes, C. A. (2006). Fabrication of hydrogen sensors with transparent titanium oxide nanotube-array thin films as sensing elements. *Thin Solid Films*, 496, 42-48, http://www.sciencedirect.com/science/article/pii/S0040609005014264.

[18] k, S.-Y., Cho, K.-K., Kim, K.-W., & Ryu, K.-S. (2010). Structure and dye-sensitized solar cell application of TiO2 nanotube arrays fabricated by the anodic oxidation method. *Phys. Scr.*, T139, 014052, http://iopscience.iop.org/1402-4896/2010/T139/014052.

[19] Tao, R.-H., Wu, J.-M., Xue, H.-X., Song, X.-M., Pan, X., Fang, X. G., Fang, X. Q., & Dai, S. Y. (2010). A novel approach to titania nanowire arrays as photoanodes of back-illu-

minated dye-sensitized solar cells. *J. Power Sources*, 195, 2989-2995, http://www.sciencedirect.com/science/article/pii/S0378775309020837.

IntechOpen